Comparison of free energy methods for molecular systems

F. Marty Ytreberg[a)]
Department of Physics, University of Idaho, Moscow, Idaho 83844-0903

Robert H. Swendsen
Department of Physics, Carnegie Mellon University, Pittsburgh, Pennsylvania 15213

Daniel M. Zuckerman[b)]
Department of Computational Biology, University of Pittsburgh, 3064 BST-3, Pittsburgh, Pennsylvania 15213

(Received 16 August 2006; accepted 6 October 2006; published online 14 November 2006)

We present a detailed comparison of computational efficiency and precision for several free energy difference (ΔF) methods. The analysis includes both equilibrium and nonequilibrium approaches, and distinguishes between unidirectional and bidirectional methodologies. We are primarily interested in comparing two recently proposed approaches, adaptive integration, and single-ensemble path sampling to more established methodologies. As test cases, we study relative solvation free energies of large changes to the size or charge of a Lennard-Jones particle in explicit water. The results show that, for the systems used in this study, both adaptive integration and path sampling offer unique advantages over the more traditional approaches. Specifically, adaptive integration is found to provide very precise long-simulation ΔF estimates as compared to other methods used in this report, while also offering rapid estimation of ΔF. The results demonstrate that the adaptive integration approach is the best overall method for the systems studied here. The single-ensemble path sampling approach is found to be superior to ordinary Jarzynski averaging for the unidirectional, "fast-growth" nonequilibrium case. Closer examination of the path sampling approach on a two-dimensional system suggests it may be the overall method of choice when conformational sampling barriers are high. However, it appears that the free energy landscapes for the systems used in this study have rather modest configurational sampling barriers. © *2006 American Institute of Physics*. [DOI: 10.1063/1.2378907]

I. INTRODUCTION

Free energy difference (ΔF) calculations are useful for a wide variety of applications, including drug design,[1,2] solubility of small molecules,[3,4] and protein/ligand binding affinities.[5–8] Due to the high computational cost of ΔF calculations, it is of interest to carefully compare the efficiencies of the various approaches.

We are particularly interested in assessing recently proposed methods[9,10] in comparison to established techniques. Thus, the purpose of this study is to provide a careful comparison of the efficiency and precision of several ΔF methods. Efficiency studies for other free energy methods include those in Refs. 11–14. We seek to answer two important questions. (i) Given a fixed amount of computational time (10^6 dynamics steps, in this study), which method estimates the correct value of ΔF with the greatest precision? (ii) Which ΔF approach can obtain a "reasonable" estimate of ΔF in the least amount of computational time?

Free energy difference methods can be classified as either equilibrium or nonequilibrium. Equilibrium approaches include multistage free energy perturbation,[15–17] thermodynamic integration,[18,19] Bennett analysis,[14,20–22] and weighted histogram analysis.[23] We term these methods "equilibrium" since all these approaches rely on fully sampled equilibrium simulations performed at each stage of the free energy calculation. Importantly, if equilibrium is not attained at each stage, then results can be biased. A host of nonequilibrium methods has recently been applied to various molecular systems, largely due to Jarzynski's remarkable equality.[24,25] Nonequilibrium methods have the potential to provide very rapid estimates of ΔF, but can also suffer from significant bias.[11,26–32]

In this report we present results using both equilibrium and nonequilibrium approaches as well as unidirectional and bidirectional methodologies. Specifically, we compare (i) adaptive integration,[9] (ii) thermodynamic integration,[18] (iii) single-ensemble path sampling of nonequilibrium work values using Jarzynski's unidirectional averaging,[10] (iv) single-ensemble path sampling using Bennett's bidirectional formalism, (v) Jarzynski averaging of nonequilibrium work values,[24,33] (vi) Bennett analysis of nonequilibrium work values,[25] (vii) equilibrium Bennett analysis,[20] and (viii) multistage free energy perturbation.[15,16] We also compare the free energy profiles, which determine the potential of mean force for adaptive integration and thermodynamic integration.

We study two test calculations: the growing and the charging of a Lennard-Jones particle in explicit water. Growth and charging can be considered as the elementary

[a)]Electronic mail: ytreberg@uidaho.edu
[b)]Electronic mail: dmz@ccbb.pitt.edu

steps in any "alchemical" free energy computation, suggesting the relevance of our results to the estimation of relative binding affinities.

Generally, one is interested in the free energy difference ($\Delta F = F_1 - F_0$) between two states or systems of interest denoted by potential energy functions $U_0(\mathbf{x})$ and $U_1(\mathbf{x})$, where $\mathbf{x}$ is the full set of configurational coordinates. ΔF can be written in terms of the partition functions for each state,

$$\Delta F = -k_B T \ln\left(\frac{Z[U_1(\mathbf{x})]}{Z[U_0(\mathbf{x})]}\right), \tag{1}$$

where k_B is the Boltzmann constant, T is the system temperature, and $Z[U(\mathbf{x})] = \int d\mathbf{x} \exp[-U(\mathbf{x})/k_B T]$. Because the overlap between U_0 and U_1 may be poor, a "path" connecting U_0 and U_1 is typically created. In our notation, the path will be parametrized using the variable λ, with $0 \leqslant \lambda \leqslant 1$.

II. EQUILIBRIUM FREE ENERGY CALCULATION

Equilibrium free energy methodologies share the common strategy of generating equilibrium ensembles of configurations at multiple values of the scaling parameter λ. In the current study we investigate thermodynamic integration,[18] adaptive integration,[9] multistage free energy perturbation,[15] and multistage equilibrium Bennett analysis.[20] We performed separate equilibrium simulations at successive values of λ, and then estimated ΔF using free energy perturbation, Bennett averaging, and thermodynamic integration on the resulting ensemble of configurations (detailed in Sec. IV).

A. Thermodynamic integration

Thermodynamic integration (TI) is probably the most common fully equilibrium ΔF approach. In TI, equilibrium simulations are performed at multiple values of λ. Then, ΔF is found by approximating the integral[18]

$$\Delta F = \int_{\lambda=0}^{1} d\lambda \left\langle \frac{\partial U_\lambda(\mathbf{x})}{\partial \lambda} \right\rangle_\lambda, \tag{2}$$

where the functional form for $U_\lambda(\mathbf{x})$ depends on the scaling methodology and will be discussed in detail in Sec. IV. The notation $\langle \cdots \rangle_\lambda$ indicates an ensemble average at a particular value of λ. In addition to the possibility of inadequate equilibrium sampling at each λ value, error arises in TI from the fact that only a finite number of λ values can be simulated, and thus the integral must be approximated by a sum.[14] Thermodynamic integration can provide very accurate ΔF calculations, but can also be computationally expensive due to the equilibrium sampling required at each λ value.[34–37]

B. Adaptive integration

The adaptive integration method (AIM), detailed in Ref. 9, seeks to estimate the same integral as that of TI, namely, Eq. (2) (see also discussions in Refs. 38–42). However, in addition to fixed-λ equilibrium sampling, the AIM approach uses a Metropolis Monte Carlo procedure to generate equilibrium ensembles for the set of λ values. The λ sampling is done by attempting Monte Carlo moves that change the value of λ during the simulation. The probability of accepting a change from the old value λ_o to a new value λ_n is

$$P_{\text{acc}}(\lambda_o \to \lambda_n) = \min[1.0, e^{-\beta(U_{\lambda_n}(\mathbf{x}) - U_{\lambda_o}(\mathbf{x}))} e^{+\beta(\delta\hat{F}(\lambda_n) - \delta\hat{F}(\lambda_o))}], \tag{3}$$

where $\beta = 1/k_B T$ and $\delta\hat{F}(\lambda_i)$ is the *current* running free energy estimate obtained by numerically approximating the integral

$$\delta\hat{F}(\lambda_i) = \int_{\lambda=0}^{\lambda_i} d\lambda \left\langle \frac{\partial U_\lambda(\mathbf{x})}{\partial \lambda} \right\rangle_\lambda. \tag{4}$$

Between attempted Monte Carlo moves in λ, any canonical sampling scheme (e.g., molecular dynamics, Langevin dynamics, and Monte Carlo) can be used to propagate the system at fixed λ. In this report, Langevin dynamics is used to sample configurations, and Monte Carlo moves in λ are attempted after every time step.

It is important to note that, due to the use of the running estimate $\delta\hat{F}$ in Eq. (3), the AIM method satisfies detailed balance only asymptotically. In other words, once the ΔF estimate fully converges, the value of $\delta\hat{F}$ is correct, and detailed balance is satisfied.[9,42]

AIM is related to parallel tempering simulation,[38] and has the associated advantage: equilibrium sampling of conformational space at one λ value can assist sampling at other λ values due to the frequent λ moves. This is reminiscent of "λ dynamics" simulation,[39,40] but contrasts with TI where only a single starting configuration is passed between λ values.

An additional advantage of AIM over the other methods detailed in this report is that there is a simple, built-in, reliable, convergence criterion. Specifically, one can keep track of the population (number of simulation snapshots) at each value of λ. When the estimate for ΔF has converged, the population will be approximately uniform across all values of λ. If the population is not approximately uniform, then the simulation should be continued.

C. Free energy perturbation

In the free energy perturbation approach, one performs independent equilibrium simulations at each λ value (like TI), then uses exponential averaging to determine the free energy difference between neighboring λ values[15]—these differences are then summed to obtain the total free energy difference. ΔF can be approximated for a path containing n λ-values (including $\lambda = 0$ and $\lambda = 1$) using the "forward" estimate [free energy perturbation—forward (FEPF)],

$$\Delta F = -k_B T \sum_{i=0}^{n-1} \ln\langle e^{-\beta(U_{\lambda_{i+1}}(\mathbf{x}_i) - U_{\lambda_i}(\mathbf{x}_i))} \rangle_{\lambda_i}, \tag{5}$$

or the "reverse" estimate [free energy perturbation—reverse (FEPR)],

$$\Delta F = +k_B T \sum_{i=0}^{n-1} \ln\langle e^{-\beta(U_{\lambda_i}(\mathbf{x}_{i+1})-U_{\lambda_{i+1}}(\mathbf{x}_{i+1})}\rangle_{\lambda_{i+1}}. \quad (6)$$

A primary limitation of free energy perturbation is that the spacing between λ values must be small enough so that there is sufficient "overlap" between the configurations spaces corresponding to λ_i or λ_{i+1}. That is, the ensemble being generated (i for forward or $i+1$ for reverse) must contain a sufficient number of conformations in all important parts of the *other* configuration space ($i+1$ or i, respectively).[11]

D. Equilibrium Bennett estimation

It is also possible to use Bennett's method to combine the information normally used for forward and reverse free energy perturbations. In this approach, one computes the free energy difference between successive λ values δF_i according to

$$\langle[1+e^{\beta(U_{\lambda_{i+1}}(\mathbf{x}_i)-U_{\lambda_i}(\mathbf{x}_i)-\delta F_i)}]^{-1}\rangle_{\lambda_i} = \langle[1+e^{\beta(U_{\lambda_{i+1}}(\mathbf{x}_{i+1})-U_{\lambda_i}(\mathbf{x}_{i+1})+\delta F_i)}]^{-1}\rangle_{\lambda i+1}. \quad (7)$$

Then the sum of these δF_i is the total free energy difference,[20]

$$\Delta F = \sum_{i=0}^{n-1} \delta F_i. \quad (8)$$

Studies have shown that using the Bennett method to evaluate free energy data is the most efficient manner to utilize two equilibrium ensembles.[14,21,22]

III. NONEQUILIBRIUM FREE ENERGY ESTIMATION

In nonequilibrium free energy approaches, the system is forced to switch to subsequent λ values, whether or not equilibrium has been reached at the current λ value. In this way, nonequilibrium paths are generated that connect U_0 and U_1. In the current study we use unidirectional Jarzynski averaging[24] and bidirectional Bennett averaging of Jarzynski-style work values,[25] as well as unidirectional[10] and bidirectional averaging of path sampled work values.

A. Jarzynski averaging

For the Jarzynski method,[24] one considers nonequilibrium paths that alternate between increments in λ and "traditional" dynamics (e.g., Monte Carlo or molecular dynamics) in $\mathbf{x}$ at fixed λ values. Thus, a path with n λ steps is given by

$$\mathbf{Z}_n = \{(\lambda_0=0,\mathbf{x}_0),(\lambda_1,\mathbf{x}_0),(\lambda_1,\mathbf{x}_1),(\lambda_2,\mathbf{x}_1), (\lambda_2,\mathbf{x}_2),\ldots,(\lambda_{n-1},\mathbf{x}_{n-1}),(\lambda_n=1,\mathbf{x}_{n-1})\}, \quad (9)$$

where it should be noted that increments (steps) from λ_i to λ_{i+1} are performed at a fixed conformation $\mathbf{x}_i$, and the initial $\mathbf{x}_0$ is drawn from the canonical U_0 distribution. For simplicity, Eq. (9) shows only a single dynamics step performed at each fixed λ_i from $\mathbf{x}_{i-1}$ to $\mathbf{x}_i$; however, multiple steps may be implemented, as below (Sec. V). A forward work value is thus given by

$$W_f(\mathbf{Z}_n) = \sum_{i=0}^{n-1} [U_{\lambda_{i+1}}(\mathbf{x}_i) - U_{\lambda_i}(\mathbf{x}_i)]. \quad (10)$$

By generating multiple paths (and thus work values) it is possible to estimate ΔF via Jarzynski's equality,[24]

$$\Delta F = -k_B T \ln\langle e^{-\beta W_f}\rangle_0, \quad (11)$$

where the $\langle\cdots\rangle_0$ represents an average over forward work values W_f generated by starting the system at U_0 and ending at U_1. A similar expression can be written for the situation when work values are generated by switching from U_1 to U_0. This approach is "unidirectional" since only work values from either forward or reverse data are used.

Perhaps the most remarkable aspect of Eq. (11) is that it is valid for arbitrary switching speed. However, in practice, the ΔF estimates are very sensitive to the distribution of work values, which in turn is largely dependent on the switching speed. Consistent with results in this report (Sec. V), other studies[13,25] have suggested that the optimal efficiency for unidirectional Jarzynski averaging is when the switching speed is slow enough that $\sigma_W \approx 1 k_B T$.

B. Bennett averaging of Jarzynski work values

Due to the bias introduced in using unidirectional Jarzynski averaging, it is useful to consider a method where both forward and reverse work values are utilized. It has been shown that the most efficient use of bidirectional data is via Bennett's method,[25,43]

$$\sum_{N_f}[1+e^{\beta(\eta+W_f-\Delta F)}]^{-1} = \sum_{N_r}[1+e^{\beta(-\eta+W_r+\Delta F)}]^{-1}, \quad (12)$$

where $\eta = k_B T \ln(N_f/N_r)$ allows for differing number of forward (N_f) and reverse (N_r) work values. Equation (12) must be solved iteratively since ΔF appears in the sum on both sides of the equation.

We note that it is also possible to extend Bennett's method to nonequilibrium free energy computation by viewing the approach as an optimized overlap sampling, which also provides a prescription for the form of U_λ.[44]

C. Single-ensemble path sampling

Single-ensemble path sampling (SEPS) is a nonequilibrium approach that seeks to generate "important" paths more frequently.[10,45–50] The method uses importance sampling to generate paths (and thus work values) according to an arbitrary distribution D, here chosen as[10]

$$D(\mathbf{Z}_n) = Q(\mathbf{Z}_n) e^{-(1/2)\beta W(\mathbf{Z}_n)}, \quad (13)$$

where $Q(\mathbf{Z}_n)$ is proportional to the probability of occurrence of an ordinary Jarzynski path and is given below. With this choice of D the free energy is estimated via (compare to (Refs. 45–49)

$$\Delta F = -k_B T \ln\left[\frac{\Sigma^D e^{-(1/2)\beta W_f}}{\Sigma^D e^{+(1/2)\beta W_f}}\right], \quad (14)$$

where the Σ^D is a reminder that the work values used in the sum must be generated according to the distribution in Eq. (13). Since forward work values, W_f are utilized in Eq. (14),

the paths must start in U_0 and end in U_1. A similar expression can be written for reverse work values W_r.

To generate work values according to the distribution D, path sampling must be used.[10,45–49,51–53] In path sampling, entire paths are generated and then accepted or rejected according to a suitable Monte Carlo criteria. In general, the probability of accepting a trial path with n λ steps ($\mathbf{Z}'_n$ with work value W') that was generated from an existing path ($\mathbf{Z}_n$ with work value W) is given by

$$P_{\text{acc}}^{\mathbf{Z}_n \to \mathbf{Z}'_n} = \min\left[1, \frac{Q(\mathbf{Z}'_n) P_{\text{gen}}^{\mathbf{Z}'_n \to \mathbf{Z}_n} e^{-(1/2)\beta W'}}{Q(\mathbf{Z}_n) P_{\text{gen}}^{\mathbf{Z}_n \to \mathbf{Z}'_n} e^{-(1/2)\beta W}}\right], \tag{15}$$

where $P_{\text{gen}}^{X \to Y}$ is the conditional probability of generating a trial path Y from existing path X.

For this study, we generate trial paths by randomly choosing a "shoot" point λ_s along an existing path (compare to Refs. 52, 54, and 55). Then, Langevin dynamics is used to propagate the system from $\lambda_s \to 0$ (backward segment), followed by $\lambda_s \to 1$ (forward segment). Before running the backward segment, the velocities at the shoot point must be reversed and then ordinary Langevin dynamics are used to propagate the system.[52] Once the trial path is complete, all the velocities for the backward segment are reversed. Since the stochastic Langevin algorithm is employed in the simulation, it is not necessary to perturb the configurational coordinates at the shoot point to obtain a trial path that differs from the existing path.

The above recipe for generating trial paths leads to the following statistical weights for the existing $Q(\mathbf{Z}_n)$ and trial $Q(\mathbf{Z}'_n)$ paths:

$$Q(\mathbf{Z}_n) = e^{-\beta U_0(\mathbf{x}_0)} \prod_{i=0}^{n-1} p(\mathbf{x}_i \to \mathbf{x}_{i+1}),$$

$$Q(\mathbf{Z}'_n) = e^{-\beta U_0(\mathbf{x}_0)} \prod_{i=0}^{n-1} p(\mathbf{x}'_i \to \mathbf{x}'_{i+1}), \tag{16}$$

where $p(\mathbf{x}_i \to \mathbf{x}_{i+1})$ is the the transition probability for taking a dynamics step from configuration $\mathbf{x}_i$ to $\mathbf{x}_{i+1}$.[55] We have assumed for simplicity that only one dynamics step is taken at each value of λ; however, the approach allows for multiple steps. The corresponding generating probabilities for the existing and trial paths are given by

$$P_{\text{gen}}^{\mathbf{Z}_n \to \mathbf{Z}'_n} = p_{\text{choose}} p_{\text{perturb}} \prod_{i=s}^{n-1} p(\mathbf{x}'_i \to \mathbf{x}'_{i+1}) \prod_{i=0}^{s-1} \bar{p}(\mathbf{x}'_{i+1} \to \mathbf{x}'_i),$$

$$P_{\text{gen}}^{\mathbf{Z}'_n \to \mathbf{Z}_n} = p'_{\text{choose}} p'_{\text{perturb}} \prod_{i=s}^{n-1} p(\mathbf{x}_i \to \mathbf{x}_{i+1}) \prod_{i=0}^{s-1} \bar{p}(\mathbf{x}_{i+1} \to \mathbf{x}_i), \tag{17}$$

where $\bar{p}(\mathbf{x}_{i+1} \to \mathbf{x}_i)$ is the transition probability of taking a *backward* step from $\mathbf{x}_{i+1}$ to $\mathbf{x}_i$. The "bar" notation is a reminder that the velocities are reversed for these segments. The probability of choosing a particular shoot point λ_s is denoted by p_{choose}, and the probability of a particular perturbation to the configurational coordinates at the shoot point is given by p_{perturb}.

Since we have chosen not to perturb the configurational coordinates at the shoot point, and any value of λ along the path is equally likely to be chosen as the shoot point, then $p_{\text{perturb}} = p'_{\text{perturb}}$ and $p_{\text{choose}} = p'_{\text{choose}}$. In addition, since the transition probabilities obey detailed balance and preserve the canonical distribution then[56]

$$\bar{p}(\mathbf{x}_{i+1} \to \mathbf{x}_i) = p(\mathbf{x}_i \to \mathbf{x}_{i+1}) e^{-\beta(U_{\lambda_{i+1}}(\mathbf{x}_i) - U_{\lambda_{i+1}}(\mathbf{x}_{i+1}))}. \tag{18}$$

Note that (18) does not contain the kinetic energy of the system, and thus is only valid for simulations done at constant temperature, such as in the current study. Inserting Eqs. (16)–(18) into Eq. (15) gives the acceptance criterion for trial paths [compare to Eq. (45) in Ref. 49]

$$P_{\text{acc}}^{\mathbf{Z}_n \to \mathbf{Z}'_n} = \min[1, e^{-\beta(\delta W - \delta W' + (1/2)(W' - W))}], \tag{19}$$

where δW is defined as the work accumulated up to the shoot point for the existing path,

$$\delta W = \sum_{i=0}^{s-1} [U_{\lambda_{i+1}}(\mathbf{x}_i) - U_{\lambda_i}(\mathbf{x}_i)] \tag{20}$$

and $\delta W'$ is the equivalent quantity for the trial path. Note that Eq. (19) is independent of the details of the fixed-λ dynamics.

To clarify ambiguities in our original presentation of the SEPS approach,[10] we also give details for applying it using overdamped Langevin dynamics (i.e., Brownian dynamics). In Ref. 10, backward segments were generated using ordinary dynamics with *negative forces*, i.e., to be very clear, the force was taken to be identical to the physical force, but opposite in sign. Thus, the transition probabilities for forward and backward steps are approximately equal,

$$\bar{p}(\mathbf{x}_{i+1} \to \mathbf{x}_i) \approx p(\mathbf{x}_i \to \mathbf{x}_{i+1}) \quad \text{(Brownian dynamics)}. \tag{21}$$

Equality occurs when the forces at $\mathbf{x}_i$ and $\mathbf{x}_{i+1}$ are identical. The acceptance criterion becomes

$$P_{\text{acc}}^{\mathbf{Z}_n \to \mathbf{Z}'_n} = \min[1, e^{-\beta((1/2)(W' - W) + U_0(\mathbf{x}'_0) - U_0(\mathbf{x}_0))}] \quad \text{(Brownian dynamics)}. \tag{22}$$

Therefore, the criticism raised in a recent paper[49] is incorrect.

D. Bennett averaging of path sampled work values

The use of bidirectional data is worth considering for the SEPS method, just as it was for ordinary nonequilibrium Jarzynski work values. Generalizing Bennett's method to include the work values sampled from D gives

$$\sum_{N_f}^{D} \frac{e^{+(1/2)\beta W_f}}{1 + e^{\beta(\eta + W_f - \Delta F)}} \left[\sum_{N_f}^{D} e^{+(1/2)\beta W_f}\right]^{-1} = \sum_{N_r}^{D} \frac{e^{+(1/2)\beta W_r}}{1 + e^{\beta(-\eta + W_r + \Delta F)}} \left[\sum_{N_r}^{D} e^{+(1/2)\beta W_r}\right]^{-1}. \tag{23}$$

Thus, to obtain a Bennett-averaged estimate for ΔF, the path

sampling algorithm is applied to generate an ensemble of paths going from U_0 to U_1 (W_f, forward) and also from U_1 to U_0 (W_r, reverse). Then, Eq. (23) is applied to the data.

IV. SIMULATION DETAILS

All alchemical mutations, such as those required for binding affinity estimation, involve changes to either the size or charge of a particle or group of particles. Thus, we chose to test the efficiency and precision of each free energy difference method detailed above using two relative solvation free energy calculations. One involves a large change in the van der Waals radius of a neutral particle in explicit solvent ("growing"), and the other is a large change in the charge of the particle while keeping the size fixed ("charging").

The system used in both cases consists of a single Lennard-Jones particle in a 24.93 Å box of 500 TIP3P water molecules. For all simulations, the molecular simulation package TINKER 4.2 was used.[57] The temperature of the system was maintained at 300.0 K using Langevin dynamics with a friction coefficient of 5.0 ps^{-1}. RATTLE was used to constrain all hydrogens to their ideal lengths,[58] allowing a 2.0 fs time step. A cutoff of 12.465 Å was chosen for electrostatic and van der Waals interactions with a smoothing function implemented from 10.465 to 12.465 Å. It is expected that the use of cutoffs will introduce systematic errors into the ΔF calculation; however, in this report we are only interested in comparing ΔF methodologies—we do not compare our results to experimental data.

For the first test case, a neutral Lennard-Jones particle was "grown" from 2.126 452 to 6.715 999 Å. The sizes were chosen to be that of lithium and cesium from the OPLS-AA force field.[59] In the second test case, the Lennard-Jones particle remains at a fixed size of 2.126 452 Å, but the charge is changed from $-e/2$ to $+e/2$. For each test case and each ΔF method, the system was initially equilibrated for 100 ps (5×10^4 dynamics steps). The initial equilibration is not included in the total computational time listed in the results; however, since every method was given identical initial equilibration times, the efficiency analysis is fair.

The λ scaling (i.e., the form of the hybrid potential U_λ) used for all ΔF methods in this study was chosen to be the default implementation within the TINKER package.[57] If a particle's charge is varied from q_0 to q_1, the hybrid potential is simply the regular potential energy calculated using a hybrid charge of

$$q_\lambda = \lambda q_1 + (1-\lambda) q_0. \tag{24}$$

Similarly, if a particle has a change in the van der Waals parameters r and ϵ the hybrid parameters are given by

$$r_\lambda = \lambda r_1 + (1-\lambda) r_0,$$

$$\epsilon_\lambda = \lambda \epsilon_1 + (1-\lambda) \epsilon_0. \tag{25}$$

The free energy slope as a function of λ for both the growing and charging test cases are shown in Figs. 1 and 3. The smoothness of both plots suggests that a more sophisticated λ scaling is not necessary for this study. If, for example, we had chosen to grow a particle from nothing, then it is likely that a different scaling would be needed (such as in Refs. 14, 36, 40, and 60).

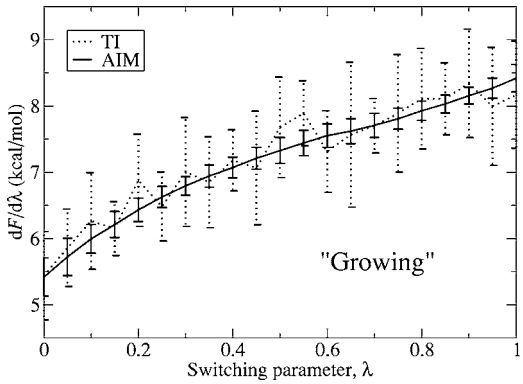

FIG. 1. The slope of the free energy $dF/d\lambda$ as a function of λ for changing the Lennard-Jones size of a neutral particle in a box of explicit water. Results for both TI and AIM methods are shown for 10^6 dynamics steps. The data show the averages (data points) and standard deviations (error bars) from 16 independent simulations for each method. The figure demonstrates that AIM has the ability to sample the λ path more efficiently, thus producing a much smoother and more precise profile compared to TI. Thus, AIM is preferred over TI for computing the potential of mean force for this system. In addition, the smoothness of the profile suggests that the switching function U_λ of Eq. (25) used in this report is adequate.

A. Thermodynamic integration calculations

For TI, equilibrium simulations were performed at each value of λ. An equal amount of simulation time was devoted to each of 21 equally spaced values of $\lambda = 0.0, 0.05, 0.1, \ldots, 0.9, 0.95$, and 1.0. Averages of the slope $dF/d\lambda = \langle dU/d\lambda \rangle_\lambda$, shown in Figs. 1 and 3, were collected for each value of λ. The first 50% of the slope data were discarded for equilibration. Finally, the data were used to estimate the integral in Eq. (2) using the trapezoidal rule. Note that higher order integration schemes were also attempted, but did not change the results, suggesting that the curves in Figs. 1 and 3 are smooth enough that high order integration schemes are not needed for this report. Also, the percentage of data that was discarded for equilibration was varied from 25% to 75% with no significant changes to the results.

B. Adaptive integration calculations

AIM results were obtained by collecting the slope of the free energy $dF/d\lambda = \langle dU/d\lambda \rangle_\lambda$ by starting the simulation from an equilibrated configuration at $\lambda = 0$ and performing one dynamics step. Immediately following the single step, a Monte Carlo move in λ was attempted, which was accepted with probability given by Eq. (3). The pattern of one dynamics step followed by one Monte Carlo trial move was repeated until a total of 10^6 dynamics steps (and thus 10^6 Monte Carlo attempts) had been performed. The same λ values used in TI are also used for AIM, thus $\lambda = 0.0, 0.05, 0.1, \ldots, 0.9, 0.95$, and 1.0 are the only allowed values. For this report Monte Carlo moves were attempted between neighboring values of λ only, i.e., a move from $\lambda = 0.35$ to 0.4 or 0.3 may be attempted but not to 0.45. Also, all $\delta\hat{F}(\lambda_i)$ values of Eq. (4) were initially set to zero. The estimate of the free energy was obtained by numerically approximating the inte-

gral in Eq. (2) using the trapezoidal rule. As with TI, higher order integration schemes did not change the results.

C. Free energy perturbation and equilibrium Bennett calculations

All free energy perturbation calculations [forward, Eq. (5), and reverse, Eq. (6)] and equilibrium Bennett computations [Eq. (8)] were performed on the same set of configurations as for TI. Specifically, equilibrium simulations were performed at each of 21 equally spaced values of $\lambda=0.0$, 0.05, 0.1, …, 0.9, 0.95, and 1.0, and the first 50% of the data were discarded for equilibration.

D. Jarzynski estimate calculations

Estimates of the free energy using the nonequilibrium work values were computed using Eq. (11) for Jarzynski averaging and Eq. (12) for Bennett averaging. Forward nonequilibrium paths were generated by starting the simulation from an equilibrated configuration at $\lambda=0$, then incrementing the value of λ, followed by another dynamics step, and so on until $\lambda=1$. Thus, only one dynamics step was performed at each value of λ. The work value associated with the path was then computed using Eq. (10). Between each path, the system was simulated for 100 dynamics steps at $\lambda=0$, starting with the last $\lambda=0$ configuration—thus the $\lambda=0$ equilibrium ensemble was generated "on the fly."

Similarly, reverse nonequilibrium paths were generated by starting each simulation from configurations in the U_1 equilibrium ensemble and switching from $\lambda=1$ to $\lambda=0$.

E. Single-ensemble path sampling calculations

For the SEPS method, we first generated an initial path using standard Jarzynski formalism. The only difference between the paths described above and the initial path for SEPS was that, due to the computer memory needed to store a path, the number of λ steps was limited to 500 for this study. In other words, if the desired path should contain around 2000 dynamics steps, the simulation would perform four dynamics steps at each λ value giving a total simulation time of 1996 dynamics steps for each path (note that simulation at $\lambda=1$ was not necessary).

Once an initial path was generated as described above, a trial path was created by perturbing the old path as described in Sec. III C. Then, the new path was accepted with probability given by Eq. (19). Importantly, if the new path was rejected, then the old path was counted again in the path ensemble. Also, as with any Monte Carlo approach, an initial equilibration phase was needed. For this report, the necessary amount of equilibration was determined by studying the dependence of the average free energy estimate, after 10^6 dynamics steps, from 16 independent trials, as a function of the number of paths that were discarded for equilibration. The optimal number of discarded paths was then chosen to be where the average free energy estimate no longer depends on the number of discarded paths.

V. RESULTS AND DISCUSSION

Using the simulation details described above, two relative solvation free energy calculations were carried out in a box of 500 TIP3P water molecules. Each of the free energy methods described above were used to estimate ΔF. Specifically, we compare:

- AIM using Eqs. (2) and (3),
- thermodynamic integration (TI) using Eq. (2),
- unidirectional SEPS using Eq. (14),
- bidirectional single-ensemble path sampling with Bennett averaging (BSEPS) using Eq. (23),
- unidirectional Jarzynski averaging of work values (Jarz) using Eq. (11),
- bidirectional Bennett averaging of Jarzynski work values (BJarz) using Eq. (12),
- equilibrium Bennett approach (Benn) using Eq. (8), and
- multistage FEPF FEPR directions using, respectively, Eqs. (5) and (6).

A. Growing a Lennard-Jones particle

We first compute the free energy required to grow a neutral particle from 2.126 452 to 6.715 999 Å in 500 TIP3P waters.

Figure 1 shows the slope of the free energy ($dF/d\lambda = \langle dU/d\lambda \rangle_\lambda$) as a function of λ for both TI and AIM after 10^6 Langevin dynamics steps. The figure suggests that AIM can more efficiently sample the profile. In AIM, configurations are not forced to remain at a particular λ, but may switch to another value of λ if it is favorable to do so. Such "cross-talk" is apparently the source of the smoother λ profile compared to TI.

Table I shows ΔF estimates for the different approaches used in this report. Note that for all nonequilibrium approaches, only the most efficient data are shown. For SEPS and BSEPS all paths were composed of 500 λ steps (restricted to 500 due to computer memory) with 40 dynamics steps at each value of λ. For Jarz and BJarz the paths were composed of 10 000 λ steps with one dynamics step at each value of λ. For all of these nonequilibrium data, the standard deviation of the work values were $\sigma_W \approx 0.8$ kcal/mol $\approx 1.3 k_B T$, in agreement with previous studies.[13,25] At least five different path lengths were attempted for each nonequilibrium method to determine the most efficient.

Table I demonstrates that, for long simulation times, all methods produce roughly the same average ΔF estimate. Also, the table clearly shows that, given 10^6 dynamics steps, AIM provides the most precise free energy estimates.

Table II shows the approximate number of dynamics steps needed by each method to obtain a free energy estimate within a specific tolerance of $\Delta F_{\text{long sim}}$ (average of all estimates at 10^6 dynamics steps). Note that the number of dynamics steps needed for the SEPS and BSEPS methods are largely due to the fact that whole paths must be discarded for

TABLE I. Free energy difference estimates in units of kcal/mol obtained for changing the Lennard-Jones size of a neutral particle in a box of explicit water. Results are shown for various methods described in the text as a function of the number of dynamics steps used in the simulation. Table entries are the mean estimates from 16 independent simulations with the standard deviation shown in parentheses. For single-ensemble path sampling (SEPS and BSEPS) and Jarzynski methods (Jarz and BJarz), only the most efficient results are shown. The table shows that in the limit of long simulation times (10^6 dynamics steps) all methods produce average ΔF estimates that roughly agree. The table also shows that AIM provides the most precise long-simulation estimate.

Steps	AIM	TI	SEPS	BSEPS	Jarz	BJarz	Benn	FEPF	FEPR
2*E*3	16.3(4.6)	16.5(6.1)	⋯	⋯	⋯	⋯	16.7(6.2)	18.7(6.7)	14.5(5.7)
4*E*3	14.4(3.9)	13.2(4.4)	⋯	⋯	⋯	⋯	13.4(4.4)	14.7(4.7)	11.9(4.2)
9*E*3	10.4(3.3)	11.2(3.6)	⋯	⋯	7.9(1.3)	⋯	11.3(3.6)	12.3(3.9)	10.1(3.3)
1.7*E*4	8.94(2.35)	9.7(2.46)	⋯	⋯	7.56(0.93)	7.53(1.13)	9.75(2.46)	10.48(2.70)	8.92(2.26)
3.5*E*4	7.51(0.52)	8.32(1.35)	⋯	⋯	7.62(0.84)	7.47(0.71)	8.36(1.38)	8.91(1.63)	7.74(1.11)
7*E*4	7.38(0.48)	7.89(1.17)	⋯	⋯	7.55(0.67)	7.38(0.59)	7.92(1.19)	8.35(1.40)	7.46(0.97)
1.3*E*5	7.35(0.36)	7.18(0.65)	7.15(0.79)	⋯	7.34(0.49)	7.36(0.38)	7.22(0.64)	7.56(0.68)	6.83(0.68)
2.7*E*5	7.34(0.23)	7.19(0.22)	7.19(0.62)	6.95(0.56)	7.35(0.44)	7.28(0.24)	7.21(0.22)	7.29(0.25)	7.08(0.20)
5.5*E*5	7.22(0.12)	7.18(0.11)	7.19(0.29)	7.12(0.46)	7.32(0.28)	7.23(0.20)	7.18(0.12)	7.22(0.11)	7.16(0.13)
1*E*6	7.19(0.07)	7.26(0.18)	7.17(0.18)	7.23(0.20)	7.25(0.23)	7.22(0.14)	7.26(0.18)	7.28(0.18)	7.24(0.20)

equilibration of the path ensemble. For all methods except AIM, the table entries for Table II were estimated using linear interpolation of the data in Table I. From the data in Table II, if the desired precision is less than 1.0 kcal/mol, then AIM, Jarz, and BJarz appear to be the best methods. However, if the desired precision is less than 0.5 kcal/mol, then AIM is the best choice.

The entropy contribution to the free energy difference $T\Delta S$ can also be estimated for growing a particle in solvent. Specifically, we use the fact that the free energy can be written as $\Delta F = \langle U \rangle_1 - \langle U \rangle_0 - T\Delta S$, where $\langle U \rangle_i$ is the average potential energy for system i. Thus, we compute $T\Delta S = -12.9 \pm 2.6$ kcal/mol, where the uncertainty for each potential energy average was estimated using the block-averaging technique[61] applied to a 2.0 ns equilibrium simulation for the system.

The large uncertainty in the entropy difference is expected due to large uncertainties in the potential energy averages $\langle U \rangle_0$ and $\langle U \rangle_1$. Note that methods for obtaining $T\Delta S$ with a lower uncertainty are possible by computing ΔF at several temperatures (see, for example, the discussion in Ref. 62). Here, the entropy difference is used only to characterize the free energy calculation, thus, we make no attempt to decrease the uncertainty in our entropy estimate.

TABLE II. Number of dynamics steps necessary to be within a specified tolerance of the correct result $\Delta F_{\text{long sim}} = 7.23$ kcal/mol, average ΔF estimate at 10^6 dynamics steps for all methods, for growing a Lennard-Jones particle in explicit solvent. The first column is the method used to obtain the estimate. The second column is the number of dynamics steps needed to estimate ΔF within 1.0 kcal/mol of $\Delta F_{\text{long sim}}$ with an uncertainty less than 1.0 kcal/mol. The third column is the number of dynamics steps needed to obtain an estimate within 0.5 kcal/mol with an uncertainty less than 0.5 kcal/mol.

Method	Within 1.0 kcal/mol	Within 0.5 kcal/mol
AIM	23 000	30 000
TI	89 000	181 000
SEPS	140 000	377 000
BSEPS	279 000	444 000
Jarz	18 000	127 000
BJarz	26 000	96 000
Benn	90 000	180 000
FEPF	104 000	191 000
FEPR	60 000	184 000

The estimated entropy difference, on its own, suggests that it may be possible to use fewer stages in our free energy computation using Benn, FEPF, and FEPR.[63] However, in these approaches, the last snapshot from a current stage is used to begin sampling at the next stage, and we found that using fewer stages increased the amount of equilibration time needed at each stage (data not shown). Thus, for this system, we did not obtain significant changes in overall efficiency by changing the number of stages.

For the current study, we have obtained converged ΔF results as indicated by the agreement between all methodologies in Table I. In the absence of such evidence, it still may be possible to gauge convergence by computing the relative entropy, as described in Refs. 31 and 32.

Thus, we conclude that, for growing a Lennard-Jones particle in explicit solvent, the preferred method depends on the type of estimate one wishes to generate. If a very precise high-quality estimate is desired, then AIM is the best choice by a considerable margin. If a very rapid estimate of ΔF, with an uncertainty of less than 1.0 kcal/mol, is desired, then comparable results are seen using AIM, Jarz, and BJarz methodologies. If the ΔF estimate is to be within 0.5 kcal/mol, then AIM is the best choice.

Finally, if the desired result is the potential of mean force, then AIM will generate a much smoother curve than TI.

1. Fast-growth unidirectional data

We now consider nonequilibrium unidirectional fast-growth data, i.e., generated by switching the system rapidly from U_0 (small particle) to U_1 (large particle). Importantly, there will be an advantage to generating unidirectional data in some cases, since only the U_0 equilibrium ensemble is needed to estimate ΔF.

In contrast to the data shown in Tables I and II, where the lengths of the nonequilibrium switching trajectories were preoptimized, here we focus on the efficacy of the methods using nonoptimal, rather fast switching. After all, when at-

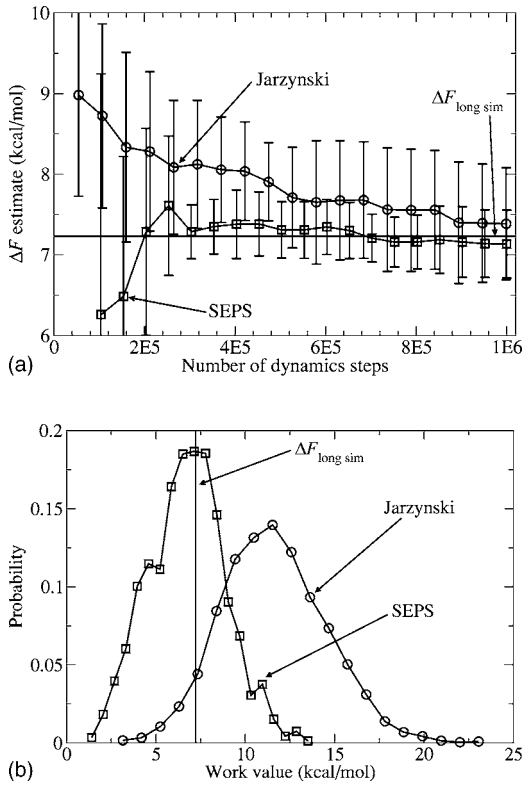

FIG. 2. (a) "Fast-growth" unidirectional free energy difference estimates obtained for changing the Lennard-Jones size of a neutral particle in a box of explicit water. Results are shown for both SEPS and Jarz methods as a function of the number of dynamics steps used in the simulation. For both methods, fast-growth work values were generated by simulating roughly 2000 dynamics steps per path, which is ten times shorter than optimal. The solid horizontal line represents the best estimate of the free energy difference $\Delta F_{\text{long sim}}$ based on averaging all results shown in Table I at 10^6 dynamics steps. The averages (data points) and standard deviations (errorbars) are from 16 independent simulations. (b) Histograms of the work values used to generate the free energy estimates for both the SEPS and Jarz methods. The plots demonstrate the potential usefulness of using path sampling over regular Jarzynski averaging. Specifically, if the work values are fast growth and unidirectional, then SEPS is able to bias the work values in such a way to improve the free energy estimate. Note that for all the SEPS data shown, the first 50 work values are thrown away for equilibration, as described in Sec. IV E.

tempting a free energy computation on a new system, there is no way to know in advance the optimal path length (number of λ steps). Substantial optimization may be needed for both SEPS and Jarz methods to work efficiently.

Here, we test the SEPS and Jarz methods using short paths with an equal number of dynamics steps. For SEPS, 500 λ steps with four dynamics steps at each value of λ were used, producing a distribution of work values with $\sigma_W = 2.1$ kcal/mol. For Jarz, 2000 λ steps with one dynamics step at each value of λ was used, producing a distribution of work values with $\sigma_W = 2.9$ kcal/mol. Note that these paths are roughly ten times shorter than optimal and thus σ_W is three to four times larger than the optimal value of $\sim k_B T$.

Figure 2 gives a comparison between SEPS and Jarz methods for the fast-growth unidirectional paths just described. The upper figure (a) shows the average free energy estimates and standard deviations for both the SEPS and Jarz methods. The lower figure (b) gives the histogram of the work values for each method. Both figures also show the

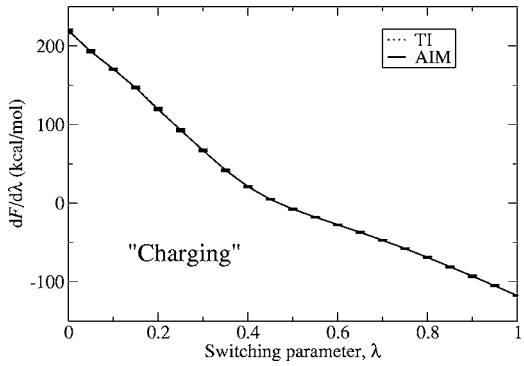

FIG. 3. The slope of the free energy $dF/d\lambda$ as a function of λ for a changing the charge of a Lennard-Jones particle in a box of explicit water from $-e/2$ to $+e/2$. Results for both TI and AIM methods are shown for 10^6 dynamics steps. The data show the averages (data points) and standard deviations (error bars) from 16 independent simulations for each method. The differences between TI and AIM are too small to resolve on the plot shown; however, it should be noted that the average uncertainty in the data for AIM is 0.38 kcal/mol and for TI is 1.05 kcal/mol, suggesting that AIM has the ability to produce a more precise profile compared to TI. Thus, AIM is preferred over TI for computing the potential of mean force for this system. The smoothness of the profile also suggests that the switching function U_λ of Eq. (24) used in this report is adequate.

"correct" value $\Delta F_{\text{long sim}}$, generated from a very long simulation. The figures clearly demonstrate that, for fast-growth data, SEPS has the ability to "shift" the work values such that the ΔF value is near the center of the work value distribution—rather than in the tail of the distribution as with the Jarz method. Thus, the SEPS results converge more rapidly than Jarz to the correct value of ΔF.

We suggest that the the SEPS method may find the greatest use for the ability to bias fast-growth work values to obtain the correct value of ΔF, as shown here.

B. Charging a Lennard-Jones particle

We next compute the free energy required to charge a particle from $-e/2$ to $+e/2$ in 500 TIP3P waters.

Figure 3 shows the slope of the free energy $(dF/d\lambda = \langle dU/d\lambda \rangle_\lambda)$ as a function of λ for both TI and AIM after 10^6 Langevin dynamics steps. The data shown in the plot are the mean (data points) and standard deviation (errorbars) for 16 independent trials. While the differences between TI and AIM are too small to resolve on the plot shown, the average uncertainty in the data for AIM is 0.38 kcal/mol and for TI is 1.05 kcal/mol, suggesting that AIM has the ability to produce more precise slope data compared to TI.

Table III shows ΔF estimates for the different approaches. For all nonequilibrium approaches, only the most efficient data are shown. For SEPS and BSEPS the paths were composed of 500 λ steps (restricted to 500 due to computer memory) with 80 dynamics steps at each value of λ. For Jarz the paths were composed of 40 000 λ steps with one dynamics step at each value of λ, and for BJarz, 20 000 λ steps with one dynamics step at each value of λ were used. For all of these nonequilibrium data, the standard deviation of the work values were $\sigma_W \approx 0.8$ kcal/mol $\approx 1.3 k_B T$, in agreement with previous studies,[13,25] and with the growing

TABLE III. Free energy difference estimates in units of kcal/mol obtained for changing the charge of a Lennard-Jones particle from $-e/2$ to $+e/2$ in a box of explicit water. Results are the averages from 16 independent simulations for various methods described in the text as a function of the number of dynamics steps used in the simulation. The standard deviation is shown in parentheses. For single-ensemble path sampling (SEPS and BSEPS) and Jarzynski methods (Jarz and BJarz), only the most efficient results are shown. The table shows that in the limit of long simulation times (10^6 dynamics steps) all methods produce average ΔF estimates that roughly agree. The table also shows that AIM and BJarz approaches provide the most precise long-simulation estimate.

Steps	AIM	TI	SEPS	BSEPS	Jarz	BJarz	Benn	FEPF	FEPR
2*E*3	8.5(5.5)	24.5(2.3)	⋯	⋯	⋯	⋯	24.4(2.3)	28.7(2.8)	20.0(2.1)
4*E*3	9.7(6.6)	21.5(3.0)	⋯	⋯	⋯	⋯	21.4(3.1)	25.4(3.0)	17.7(3.1)
9*E*3	14.6(11.4)	20.1(1.7)	⋯	⋯	⋯	⋯	20.1(1.8)	22.6(1.8)	17.6(2.1)
1.7*E*4	18.6(10.8)	18.5(1.2)	⋯	⋯	⋯	⋯	18.5(1.2)	20.3(1.1)	16.8(1.4)
3.5*E*4	19.7(4.6)	18.44(0.87)	⋯	⋯	19.15(0.70)	18.42(0.74)	18.39(0.90)	19.56(1.05)	17.34(0.70)
7*E*4	18.42(0.43)	18.38(0.69)	⋯	⋯	18.82(0.61)	18.29(0.40)	18.33(0.69)	19.18(0.87)	17.64(0.69)
1.3*E*5	18.41(0.26)	18.34(0.71)	⋯	⋯	18.72(0.55)	18.20(0.46)	18.28(0.72)	18.76(0.83)	17.78(0.80)
2.7*E*5	18.27(0.21)	18.35(0.45)	18.47(1.03)	18.23(0.59)	18.55(0.42)	18.16(0.29)	18.29(0.45)	18.62(0.54)	18.09(0.46)
5.5*E*5	18.26(0.13)	18.28(0.28)	18.25(0.49)	18.43(0.43)	18.44(0.32)	18.13(0.19)	18.20(0.29)	18.28(0.39)	18.25(0.26)
1*E*6	18.23(0.13)	18.28(0.30)	18.23(0.30)	18.30(0.42)	18.32(0.26)	18.18(0.16)	18.21(0.31)	18.20(0.33)	18.25(0.31)

data in this study. At least four different path lengths were attempted for each nonequilibrium method to determine the most efficient.

Table III demonstrates that, for long simulation times, all methods produce roughly the same average ΔF estimate. Also, the table shows that, given 10^6 dynamics steps, AIM and BJarz methodologies provide the most precise free energy estimates.

Using the same procedure as for the growing problem above, we estimate the entropy contribution to the free energy difference as $T\Delta S=6.9\pm3.5$ kcal/mol. Again, although the small entropy contribution suggests that it may be possible to use fewer stages in Benn, FEPF, and FEPR calculations,[63] we found that using fewer stages increases the amount of equilibration time needed at each stage (data not shown), and thus efficiency was not significantly affected by this type of change in staging.

For fast estimation of free energy differences, Table IV shows the number of dynamics steps needed by each method to obtain a free energy estimate within a specific tolerance of $\Delta F_{\text{long sim}}$ (average of all estimates at 10^6 dynamics steps).

TABLE IV. Number of dynamics steps necessary to be within a specified tolerance of the correct result $\Delta F_{\text{long sim}}=18.24$ kcal/mol, average ΔF estimate at 10^6 dynamics steps for all methods, for charging a Lennard-Jones particle in explicit solvent. The first column is the method used to obtain the estimate. The second column is the number of dynamics steps needed to estimate ΔF within 1.0 kcal/mol of $\Delta F_{\text{long sim}}$ with an uncertainty less than 1.0 kcal/mol. The third column is the number of dynamics steps needed to obtain an estimate within 0.5 kcal/mol with an uncertainty less than 0.5 kcal/mol.

Method	Within 1.0 kcal/mol	Within 0.5 kcal/mol
AIM	52 000	64 000
TI	27 500	243 000
SEPS	291 000	515 000
BSEPS	399 000	487 000
Jarz	40 000	180 000
BJarz	40 000	69 000
Benn	29 000	245 000
FEPF	43 000	335 000
FEPR	26 000	252 000

Note that the number of dynamics steps needed for the SEPS and BSEPS methods is large due to the fact that many paths must be discarded for equilibration of the path ensemble. For all methods except AIM, the entries in Table IV were estimated using linear interpolation of the data in Table III. From the data in the table, if the desired precision is less than 1.0 kcal/mol, then all methods other than SEPS and BSEPS produce comparable results. However, if the desired precision is less than 0.5 kcal/mol, then AIM and BJarz approaches are best.

We conclude that, when charging a Lennard-Jones particle in explicit solvent, the preferred methodology depends on the type of estimate one wishes to generate. If a very high quality estimate is desired, then AIM is the best choice, closely followed by BJarz. If a very rapid estimate of ΔF, with an uncertainty of less than 1.0 kcal/mol, is desired, then comparable results are seen using all methodologies *except* for SEPS and BSEPS. If the ΔF estimate is to be within 0.5 kcal/mol, then AIM and BJarz are the best choices.

Finally, if the desired result is the potential of mean force, then AIM will generate a much smoother curve than TI.

C. A second look at a two-dimensional model

Because SEPS proved orders of magnitude more efficient than TI and Jarz in the study of a two-dimensional model,[10] we return to that model in an effort to understand the decreased effectiveness of SEPS in the present study. Specifically, we use the model from Ref. 10, but now for a wide range of conformational sampling barrier heights (fixed λ), and then compare SEPS to TI, as in our original study. Note, that we use the term "conformational sampling barrier" to distinguish it from the barrier in λ space.

Some alterations to our approach in Ref. 10 were necessary to provide a fair comparison in the context of the present report. The results in Ref. 10 were obtained for very short paths, large perturbations of the shoot point, and a conformational sampling barrier height of $14.0k_BT$ in U_1. For consistency with the present studies, SEPS results were generated with *no* perturbation of the shoot point, much longer

TABLE V. Number of dynamics steps necessary to be within $0.5k_BT$ of the analytical result for ΔF with a $0.5k_BT$ or less standard deviation for the two-dimensional model in Ref. 10. The first column is the barrier height of the potential energy surface in k_BT units. The second and third columns are the total numbers of dynamics steps using SEPS with, respectively, 200 work values and 20 000 work values. The fourth column is the total number of dynamics steps using TI with using 51 equally spaced values of λ. For both TI and SEPS, half of the generated data was thrown away for equilibration.

Barrier (k_BT)	SEPS long	SEPS short	TI
1.0	60 000	200 000	15 300
2.0	120 000	500 000	35 700
4.0	400 000	1 000 000	204 000
6.0	1 400 000	1 400 000	1 020 000
8.0	8 000 000	1 600 000	5 100 000
10.0	40 000 000	2 400 000	20 400 000
12.0	80 000 000	4 000 000	76 500 000
14.0	200 000 000	10 000 000	204 000 000

paths, and for a range of conformational sampling barrier heights. Both TI and SEPS simulations utilized Brownian dynamics to propagate the system. For SEPS, paths were generated as described in the present report (but with no velocity), and accepted with the probability given in Eq. (19).

For completeness, we give the two-dimensional potential used:[10] $U_0(x,y)=(x+2)^2+y^2$ and $U_1(x,y)=(A/10)\{((x-1)^2-y^2)^2+10(x^2-5)^2+(x+y)^4+(x-y)^4\}$, where A is varied to change the height of the barrier for U_1. Note that there is only one barrier, which is parallel to the y axis, and all paths must necessarily cross this barrier to get from one well to the other (see Ref. 10).

Results for the two-dimensional model using SEPS and TI are shown in Table V. The free energy change is for switching between a single-well potential and a double-well potential with a conformational barrier height in k_BT units given in the first column. The next three columns give the total numbers of dynamics steps needed for the ΔF estimate to be within $0.5k_BT$ of the correct value with $0.5k_BT$ or smaller standard deviation (estimated over at least 100 trials): the second and third columns are for SEPS where either 200 (long trajectories) or 20 000 (short trajectories) work values were generated with 50% of the work values discarded for equilibration, and the fourth column is TI using 51 evenly spaced values of λ with 50% of the data at each value of λ discarded for equilibration.

Table V clearly shows that, for very low conformational barrier height, TI is much more efficient than SEPS, and that the most efficient SEPS is obtained using longer paths and thus fewer work values. For increasing conformational barrier heights, SEPS using long paths and TI become comparable, while SEPS using short paths becomes the most efficient. For the largest conformational barrier height tested in this study ($14.0k_BT$), SEPS using short paths is at least 20 times more efficient than either TI or SEPS using long paths.

Since the results for growing and charging an ion in solvent showed that TI was more efficient than SEPS, we suggest that the free energy landscapes for the molecular systems used in this study have rather modest conformational sampling barriers.[64,65]

VI. CONCLUSIONS

We have carefully studied several computational free energy difference (ΔF) methods, comparing efficiency and precision. The test cases used for the comparison were relative solvation energy calculations involving either a large change in the Lennard-Jones size or in the charge of a particle in explicit solvent. Specifically, we compared adaptive integration method (AIM), thermodynamic integration (TI), path sampling of nonequilibrium work values using both a Jarzynski unidirectional formalism (SEPS) and a Bennett-type bidirectional formalism (BSEPS), Jarzynski (Jarz) and Bennett (BJarz) averaging of nonequilibrium work values, equilibrium Bennett (Benn), and free energy perturbation (forward, FEPF, and reverse, FEPR).

AIM (Ref. 9) was found to provide very high quality, precise estimates, given long simulation times (10^6 total dynamics steps in this study), and also allowed very rapid estimation of ΔF. In addition, AIM provided smooth free energy profiles (and thus smooth potential of mean force curves) as compared to TI: (see Figs. 1 and 3). Clearly, AIM was the best all-around choice for the systems studied here.

BJarz (Ref. 25) was also found to perform very well, with long-simulation results that were second only to AIM. However, it should be noted that the data shown in this study are for the most efficient path lengths only. To determine the optimal path length, many simulations were performed, adding to the overall cost of the method. Also, our results showed that using bidirectional data (BJarz) produced considerably more precise results than using unidirectional data (Jarz).

The SEPS method[10] is shown to provide accurate free energy estimates from "fast-growth" unidirectional nonequilibrium work values. Specifically, in cases where the standard deviation of the work values is much greater than k_BT ($\sigma_W \gg k_BT$), the SEPS method can effectively shift the work values to allow for more accurate ΔF estimation than is possible using ordinary Jarzynski averaging. Interestingly, using bidirectional data (BSEPS) did not increase the precision of the ΔF estimate, and perhaps made it somewhat worse.

We also find, in agreement with previous studies,[13,25] that the greatest efficiency for the Jarz approach is when $\sigma_W \approx 1k_BT$. For the first time, we also show that SEPS is also most efficient when $\sigma_W \approx 1k_BT$ for the molecular systems studied in this report.

We have also suggested an explanation—with potentially quite interesting consequences—for the decreased effectiveness of SEPS in molecular systems. By reexamining the two-dimensional model used in our first SEPS paper,[10] we find that SEPS can indeed be much more more efficient than TI, but *only when the conformational sampling barrier is very high* ($\gg k_BT$). This suggests that the configurational sampling barriers encountered in the molecular systems studied here are fairly modest, counter to our own expectations. A key question is thus raised. How high are conformational

sampling barriers encountered in free energy calculations of "practical interest?" (See also Refs. 64 and 65.)

We remind the reader that the specific results of this study are valid only for the types of ΔF calculations we considered, namely, growing and charging a Lennard-Jones particle in explicit solvent. However, we believe the results should prove pertinent to an array of alchemical computations built from the types of "elementary" changes we considered. We also believe the results may have bearing on other types of free energy calculations in molecular systems characterized by modest conformational sampling barriers, as were apparently present in our studies.

ACKNOWLEDGMENTS

The authors would like to thank Ron White and Hagai Meirovitch for valuable discussions, and also Manuel Athènes and Gilles Adjanor for helpful comments regarding the manuscript. Funding for this research was provided by the Department of Computational Biology and the Department of Environmental and Occupational Health at the University of Pittsburgh, and the National Institutes of Health under Fellowship No. GM073517 [to one of the authors (F.M.Y.)] and Grant Nos. ES007318, GM073517, and CA078039.

[1] W. L. Jorgensen, Science **303**, 1813 (2004).
[2] C. Sotriffer, G. Klebe, M. Stahl, and H.-J. Bohm, *Burger's Medicinal Chemistry and Drug Discovery*, 6th ed. (Wiley, New York, 2003), Vol. 1.
[3] J. W. Pitera and W. F. van Gunsteren, J. Phys. Chem. B **105**, 11264 (2001).
[4] A. Grossfield, P. Ren, and J. W. Ponder, J. Am. Chem. Soc. **125**, 15671 (2003).
[5] S. B. Singh, Ajay, D. E. Wemmer, and P. A. Kollman, Proc. Natl. Acad. Sci. U.S.A. **91**, 7673 (1994).
[6] B. C. Oostenbrink, J. W. Pitera, M. M. van Lipzip, J. H. N. Meerman, and W. F. van Gunsteren, J. Med. Chem. **43**, 4594 (2000).
[7] H. Fujitani, Y. Tanida, M. Ito, G. Jayachandran, C. D. Snow, M. R. Shirts, E. J. Sorin, and V. S. Pande, J. Chem. Phys. **123**, 084108 (2005).
[8] Y. Deng and B. Roux, J. Chem. Theory Comput. **2**, 1255 (2006).
[9] M. Fasnacht, R. H. Swendsen, and J. M. Rosenberg, Phys. Rev. E **69**, 056704 (2004).
[10] F. M. Ytreberg and D. M. Zuckerman, J. Chem. Phys. **120**, 10876 (2004); **121**, 5022 (2004).
[11] D. A. Kofke and P. T. Cummings, Mol. Phys. **92**, 973 (1997).
[12] R. J. Radmer and P. A. Kollman, J. Comput. Chem. **18**, 902 (1997).
[13] G. Hummer, J. Chem. Phys. **114**, 7330 (2001).
[14] M. R. Shirts and V. S. Pande, J. Chem. Phys. **122**, 144107 (2005).
[15] R. W. Zwanzig, J. Chem. Phys. **22**, 1420 (1954).
[16] J. P. Valleau and D. N. Card, J. Chem. Phys. **57**, 5457 (1972).
[17] G. M. Torrie and J. P. Valleau, J. Comput. Phys. **23**, 187 (1977).
[18] J. G. Kirkwood, J. Chem. Phys. **3**, 300 (1935).
[19] T. P. Straatsma and J. A. McCammon, J. Chem. Phys. **95**, 1175 (1991).
[20] C. H. Bennett, J. Comput. Phys. **22**, 245 (1976).
[21] N. Lu, J. K. Singh, and D. A. Kofke, J. Chem. Phys. **118**, 2977 (2003).
[22] N. Lu, D. A. Kofke, and T. B. Woolf, J. Comput. Chem. **25**, 28 (2004).
[23] S. Kumar, J. M. Rosenberg, D. Bouzida, R. H. Swendsen, and P. A. Kollman, J. Comput. Chem. **13**, 1011 (1992).
[24] C. Jarzynski, Phys. Rev. Lett. **78**, 2690 (1997).
[25] G. E. Crooks, Phys. Rev. E **61**, 2361 (2000).
[26] F. M. Ytreberg and D. M. Zuckerman, J. Comput. Chem. **25**, 1749 (2004).
[27] D. M. Zuckerman and T. B. Woolf, Phys. Rev. Lett. **89**, 180602 (2002).
[28] N. Lu and D. A. Kofke, J. Chem. Phys. **114**, 7303 (2001).
[29] N. Lu and D. A. Kofke, J. Chem. Phys. **115**, 6866 (2001).
[30] J. Gore, J. Ritort, and C. Bustamante, Proc. Natl. Acad. Sci. U.S.A. **100**, 12564 (2003).
[31] D. Wu and D. A. Kofke, J. Chem. Phys. **123**, 084109 (2005).
[32] D. Wu and D. A. Kofke, J. Chem. Phys. **123**, 054103 (2005).
[33] C. Jarzynski, Phys. Rev. E **56**, 5018 (1997).
[34] S. Boresch, F. Tettinger, M. Leitgeb, and M. Karplus, J. Phys. Chem. B **107**, 9535 (2003).
[35] T. Z. Mordasini and J. A. McCammon, J. Phys. Chem. B **104**, 360 (2000).
[36] M. R. Shirts, J. W. Pitera, W. C. Swope, and V. S. Pande, J. Chem. Phys. **119**, 5740 (2003).
[37] T. P. Lybrand, I. Ghosh, and J. A. McCammon, J. Am. Chem. Soc. **107**, 7793 (1985).
[38] E. Marinari and G. Parisi, Europhys. Lett. **19**, 451 (1992).
[39] B. Tidor, J. Phys. Chem. **39**, 1069 (1993).
[40] X. Kong and C. L. Brooks, J. Chem. Phys. **105**, 2414 (1996).
[41] F. Wang and D. P. Landau, Phys. Rev. Lett. **86**, 2050 (2001).
[42] D. J. Earl and M. W. Deem, J. Phys. Chem. B **109**, 6701 (2005).
[43] M. R. Shirts, E. Bair, G. Hooker, and V. S. Pande, Phys. Rev. Lett. **91**, 140601 (2003).
[44] N. Lu, D. Wu, T. B. Woolf, and D. A. Kofke, Phys. Rev. E **69**, 057702 (2004).
[45] S. X. Sun, J. Chem. Phys. **118**, 5769 (2003).
[46] E. Atilgan and S. X. Sun, J. Chem. Phys. **121**, 10392 (2004).
[47] M. Athènes, Phys. Rev. E **66**, 046705 (2002).
[48] M. Athènes, Eur. Phys. J. B **38**, 651 (2004).
[49] G. Adjanor and M. Athènes, J. Chem. Phys. **123**, 234104 (2005).
[50] D. Wu and D. A. Kofke, J. Chem. Phys. **122**, 204104 (2005).
[51] L. R. Pratt, J. Phys. Chem. **85**, 5045 (1986).
[52] P. G. Bolhuis, D. Chandler, C. Dellago, and P. L. Geissler, Annu. Rev. Phys. Chem. **53**, 291 (2002).
[53] G. Hummer, J. Chem. Phys. **120**, 516 (2004).
[54] C. Dellago, P. G. Bolhuis, and D. Chandler, J. Chem. Phys. **110**, 6617 (1999).
[55] C. Dellago, P. G. Bolhuis, F. S. Csajka, and D. Chandler, J. Chem. Phys. **108**, 1964 (1998).
[56] C. Dellago, P. G. Bolhuis, and D. Chandler, J. Chem. Phys. **108**, 9236 (1998).
[57] J. W. Ponder and F. M. Richard, J. Comput. Chem. **8**, 1016 (1987); http://dasher.wustl.edu/tinker
[58] H. C. Andersen, J. Comput. Phys. **52**, 24 (1983).
[59] W. L. Jorgensen, D. S. Maxwell, and J. Tirado-Rives, J. Am. Chem. Soc. **117**, 11225 (1996).
[60] W. Yang, R. Bitetti-Putzer, and M. Karplus, J. Chem. Phys. **120**, 2618 (2004).
[61] H. Flyvbjerg and H. G. Petersen, J. Chem. Phys. **91**, 461 (1989).
[62] S. Wan, R. H. Stote, and M. Karplus, J. Chem. Phys. **121**, 9539 (2004).
[63] N. Lu and D. A. Kofke, J. Chem. Phys. **111**, 4414 (1999).
[64] R. Elber and R. Czerminski, J. Chem. Phys. **92**, 5580 (1990).
[65] D. M. Zuckerman and E. Lyman, J. Chem. Theory Comput. **2**, 1200 (2006) (erratum in press).